Article ID: 1003 - 6326(1999)04 - 0733 - 08

Solder joint geometry of tin-lead alloy and its application in electronic packaging①

Wang Guozhong(王国忠)[1], Zhu Qinong(朱其农)[1], Cheng Zhaonian(程兆年)[1]
Wang Chunqing(王春青)[2], Qian Yiyu(钱乙余)[2]
1. *Shanghai Institute of Metallurgy, The Chinese Academy of Sciences, Shanghai 200050, P.R. China;*
2. *Harbin Institute of Technology, Harbin 150001, P.R. China*

Abstract: By employing the minimum energy theorem, the potential energy controlling equation, which consists of surface energy and gravitational energy for molten meniscus, was investigated. The solder joint geometry of molten tin-lead solder alloy for chip component and thin quad flat package were simulated with finite element method. The simulation results of solder joint geometry are coincident well with the experimental results. The solder joint geometry was applied to study the solder joint reliability for chip component RC3216. The thermal cycling tests revealed that the solder joint geometry plays an important role in solder joint reliability.

Key words: tin-lead solders; solder joint geometry; simulation; thermal cycling life
Document code: A

1 INTRODUCTION

In materials science and engineering, many phenomena and properties depend on the shape of interfaces and surfaces, stability and associated potentials. In the fields of electronic packaging and surface mount technology, the high density and high reliability are the current needs and the future trends. The reliability and the manufacturing process of tin-lead (SnPb) based solder joint are the essential problems of electronic packaging industry. Previous researches[1,2] have proved that the solder joint geometry plays an important role in solder joint reliability. In the manufacturing process of package and assembly with high I/O pins and high density, there exists a problem how to determine the solder volume to obtain the high quality identical solder joint. Moreover, the inspection and rework are extremely diffcult for fine pitch package and assembly techniques. Therefore, the numerical simulation and manufacturing control of solder joint geometry has received more attentions in recent years[3~6]. The authors have already investigated the solder joint geometry for several types of electronic package[7,8].

This paper is to establish numerical simulation method of tin-lead solder joint geometry, the solder joint geometry of chip component and thin quad flat package were simulated with finite element method. As an application example, the solder joint geometry was applied to the study of solder joint reliability for chip component RC3216.

2 MATHEMATICAL FORMULATION

2.1 Solder joint formation

When solid, gaseous and liquid phases coexist, the liquid wets and spreads along the solid surface, a meniscus forms and the contact angle (θ) occurs at the point of triple phases. In the problem of solder joint formation, the solder alloy (in paste form for reflow soldering process) is heated until liquefied, the molten solder then wets and spreads along the metal surfaces at the

① Received Sep. 17, 1998; accepted Feb. 3, 1999

conjunction, and reacts with metals through dissolution and diffusion, etc. Finally it is cooled to form the solid joint to fulfill electrical, thermal and mechanical interconnections between the electronic package and the substrate, such as glass/epoxy FR4 and Al_2O_3 ceramic. The solder joint formation is an essential problem of electronic packaging and assembly technologies, and is a complex physical/chemical process interrelated with the fluid flow, heat transfer, phase transform, etc. The solder joint geometry refers to the final geometry of the solder after the reflow soldering, that is the size molten solder can reach by wetting and spreading along metal surfaces, the contact angles and the solder fillet shapes.

2.2 Physical model

2.2.1 Assumptions

For the purpose of simplicity and effective simulation of solder joint geometry in good precision, two basic assumptions are considered. First, by employing the minimum energy theorem, the final solder joint geometry after reflow soldering is considered the quasi-static equilibrium (thermal and chemical) shape of the molten solder formed at the conjunction. Second, the limiting metallizations of package and substrate pad introduce finite spreading of molten solder. In the numerical simulation of 3-D solder joint geometry presented below, the following assumptions are implicit:

1) The effects of composition change in molten solder, resulting from metal diffusion and dissolution, on the physical properties (density ρ, surface tension γ) are neglected;

2) There is no temperature gradient over all the solder joint during reflow soldering, so the Marangoni effect[9] is neglected, i.e. the density and surface tension of molten solder are uniform;

3) The formation of metal oxidation film and the change of flux activity have no effects on the solder joint formation;

4) The volume shrinkage of solder($\sim$3%) during cooling process is negligible.

2.2.2 Potential energy of solder joint system

On the above assumptions, the solder joint geometry is the equilibrium meniscus of molten solder at the conjunction, which minimizes the total potential energy. The potential energy (E) which governs the solder joint geometry in the present study includes a surface energy term (E_S) and a gravitational energy term (E_G)

$$E = E_S + E_G \tag{1}$$

The surface energy can be derived as

$$E_S = \iint \gamma' \mathrm{d}A \tag{2}$$

where γ' is the surface tension between two phases, and A is the area. The surface energy corresponding to the interface along substrate pad and solderable metallization of electronic package depends on the wetting angles, i.e., the equilibrium contact angles, when the wetting and spreading of the molten solder does not reach the finite dimensions. Applying Young's equation at the triple point and dropping the constant energy terms, Eq. (2) can be rewritten as

$$E_S = \iint_{A_0} \gamma \mathrm{d}A + \iint_{A_1} -\gamma\cos\theta_1 \mathrm{d}A + \iint_{A_2} -\gamma\cos\theta_2 \mathrm{d}A \tag{3}$$

where γ is the surface tension of molten solder, A_0, A_1 and A_2 are the interface areas between molten solder and gas, pad metallization and package metallization, θ_1 and θ_2 are the wetting angles of molten solder on metallization surfaces of pad and package, respectively.

Since the package and substrate are fixed, their gravitational energies are constant and can be dropped. then the gravitational energy of the solder joint system consists only of term for molten solder and can be derived as

$$E_G = \iiint_V \rho g z \mathrm{d}V \tag{4}$$

where ρ is the density of molten solder, g is the gravitational acceleration, z is the height coordinate, and V is the solder volume, respectively. Thus, the minimum potential energy which governs the solder joint geometry can be written as follows:

$$\min E = \min[\iint_{A0} \gamma \mathrm{d}A + \iint_{A1} -\gamma\cos\theta_1 \times \mathrm{d}A + \iint_{A2} -\gamma\cos\theta_2 \mathrm{d}A + \iiint_V \rho g z \mathrm{d}V \tag{5}$$

The volume integral form of constant volume condition (V_0) is given as

$$V_0 = \iiint_V \mathrm{d}V \tag{6}$$

By using the finite element method for variation problem, the quasi-static equilibrium geometry of the molten solder can then be solved.

2.3 Method of solution

The steps for implementing the finite element method for determining the solder joint geometry are given in the following.

(1) Develop the integral forms of potential energies which govern the solder joint formation. In addition, the boundary conditions and the fixed solder volume constraint should also be defined.

(2) Discretize the interfaces and surfaces with finite elements, e.g. the three dimensional surface is implemented as a simplex, that is, a union of triangular elements.

(3) Transform all integrals for energies and volume into surface integrals and boundary integrals.

(4) Select the suitable shape function, i.e., interpolation functions, to expand the spatial variables over each finite element in a parameteric form involving the element nodal coordinates. That is,

$$\bar{r}^{(e)} = \sum_{i=1}^{3} (\alpha_i \bar{r}_i^{(e)} + \beta_i \bar{r}_{i,\xi}^{(e)} + r_i \bar{r}_{i,\eta}^{(e)}) \tag{7}$$

where $\bar{r}_i^{(e)}$, $\bar{r}_{i,\xi}^{(e)}$ and $\bar{r}_{i,\eta}^{(e)}$ are element nodal coordinates and their partial derivatives; α_i, β_i, and γ_i are interpolation functions; $\bar{r}^{(e)}$ are the spatial variables which define the surface, and $e = 1, 2, \cdots, m$, m is the total number of elements, respectively.

(5) Use the fitting arithmetic to determine the remaining unknown nodal coordinates by minimizing the potential energies subject to the boundary conditions and the fixed volume constraint.

In the present work, the Surface Evolver program[10], which is an interactive program for study of surfaces shaped by surface tension and other energies, is applied to solve the solder joint formation. The triangular element facet (denoted as f) consists of vertices (denoted as v) and edges (denoted as s). The coordinates of the vertices are the parameters that determine the location of the surface and are changed when the surface evolves. An edge is an oriented line segment between a tail vertex and a head vertex. The element is defined as

$$f = \frac{1}{2} \left\| \boldsymbol{s}_1 \times \boldsymbol{s}_2 \right\| \cdot \boldsymbol{n} \tag{8}$$

where $\boldsymbol{n}$ is the mormal unit vector of the element. The surface energy ($E_S^{(e)}$) and gravitational energy ($E_G^{(e)}$) of the element can be derived as

$$E_S^{(e)} = \frac{\gamma}{2} \left\| \boldsymbol{s}_1 \times \boldsymbol{s}_2 \right\| \tag{9}$$

$$E_G^{(e)} = \frac{1}{24}\rho g(z_1^2 + z_2^2 + z_3^2 + z_1 z_2 + z_2 z_3 + z_1 z_3)(\boldsymbol{k} \cdot \boldsymbol{s}_1 \times \boldsymbol{s}_2) \tag{10}$$

where $z_i (i = 1, 2, 3)$ are the coordinates of the vertex. The forces acting on the vertex resulting from the surface energy and gravitational energy are written as follows:

$$\boldsymbol{F}(E_S) = \frac{\gamma}{2} \cdot \frac{\boldsymbol{s}_2 \times (\boldsymbol{s}_1 \times \boldsymbol{s}_2)}{\left\| \boldsymbol{s}_1 \times \boldsymbol{s}_2 \right\|} \tag{11}$$

$$\boldsymbol{F}(E_G) = -\frac{1}{24}[(2z_1 + z_2 + z_3)(\boldsymbol{k} \cdot \boldsymbol{z}_1 \times \boldsymbol{z}_2) + (z_1^2 + z_2^2 + z_3^2 + z_1 z_2 + z_2 z_3 + z_1 z_3)(\boldsymbol{k} \times \boldsymbol{s}_2)] \tag{12}$$

During the iteration, each vertex is simultaneously forced to move in direction of the force on the vertex. Then the shape and the spatial location of the element are changed, and finally the surface is evolved towards minimal energy.

3 EXPERIMENTAL

3.1 Contact angle

In order to implement the proposed model in a practical setting, some basic physical properties for molten solder, such as density, surface tension, and wetting angle at the triple point must be available. Values of density and surface tension of molten eutectic solder can be calculated[11] or available in the literature[12]. The wetting angle can be determined by experimentation.

In this paper, the contact angles of eutectic

60Sn40Pb solder on Cu metallization layer, which is the most common metallization layer on glass/epoxy FR4 substrate, were experimentally investigated. The experimental results of contact angles during soldering process are shown in Fig. 1. It is seen that the contact angle decreases with the increase of soldering temperature and soldering time. When the soldering process continues and nearly reaches its quasi-static state, the contact angle decreases slightly, and at that time the contact angle (~15°) is nearly the wetting angle. If the soldering process is held for a long period of time, the phenomenon of dewetting can occur. The contact angle then conversely increases over time due to the contract of molten solder on the metal surface, which is resulted from the formation of intermediate compounds (Cu_xSn_y) and the over-dissolution of the metallization layer into the molten solder.

The exponent Arrihenius function was applied to regress the experimental data of the contact angle:

$$\theta = \theta_0[t\exp(-Q/RT)]^n \quad (13)$$

where θ_0 is a constant, R is the gas constant, T is the absolute temperature, n is the exponent, and Q is the activation energy, respectively. The determined parameters are: $\theta_0 = 0.0796$, $n = -0.3$, and $Q = 90.3$ kJ/mol. The activation energy can be comprehended as the activation energy of wetting and spreading of molten solder on the metal surface. The value of Q is nearly the activation energy of self-diffusion

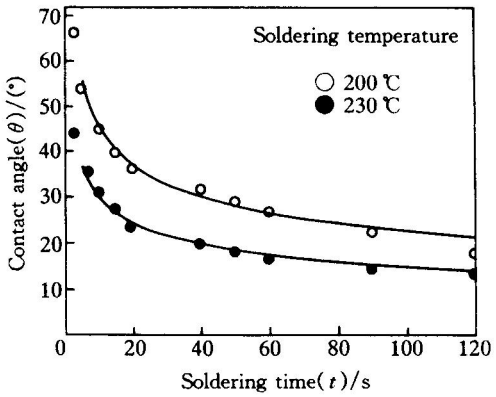

Fig. 1 Relationship between contact angle and reflow soldering process

for Sn and Pb atoms: $Q_{Sn} = 93.6$ kJ/mol[13]. It is indicated that the wetting process of molten SnPb solder is correlated with the diffusions of Sn and Pb atoms. From the above results, for the near equilibrium vapor phase reflow soldering where temperature is 215 ℃ and soldering time is usually about 2 min, the wetting angle of eutectic molten solder on Cu metal surface can be determined as 15°.

3.2 Solder joint geometry

A leadless chip component RC3216 was selected to be surface mounted on FR4 substrate with eutectic solder to form the solder joint geometry. By following the procedure: solder paste printing, chip placing and vapor phase reflow soldering, the solder joints were obtained. Fig. 2 shows the typical micrographs of an actual castellated solder joint geometry. The measurement method of solder joint geometry by using a touch pin, which slides slightly along the fillet surface, is applied to gain the height variations (z direction) of solder fillet profiles in two directions equidistantly, one is along the joint width (x direction), the other the joint length (y direction). Fig. 3 shows the experimental results of the solder joint geometry.

It is seen that the solder joint geometry is spatial curved surface, the cross-section profile of the solder fillet varies along the joint length and width. Moreover, the experimental results (no figures in this paper) show that the solder fillet shape can be varied from concave to convex by increasing the solder volume or decreasing the pad length. The stand-off height between chip component and the substrate also affects the solder joint geometry effectively. From the above results, the solder joint geometry can be designed and controlled along the manufacturing parameters.

4 SIMULATION OF SOLDER JOINT GEOMETRY

4.1 Input parameters

The solder joint geometry was determined with these input parameters: dimensions of metallizations of substrate pad and electronic package

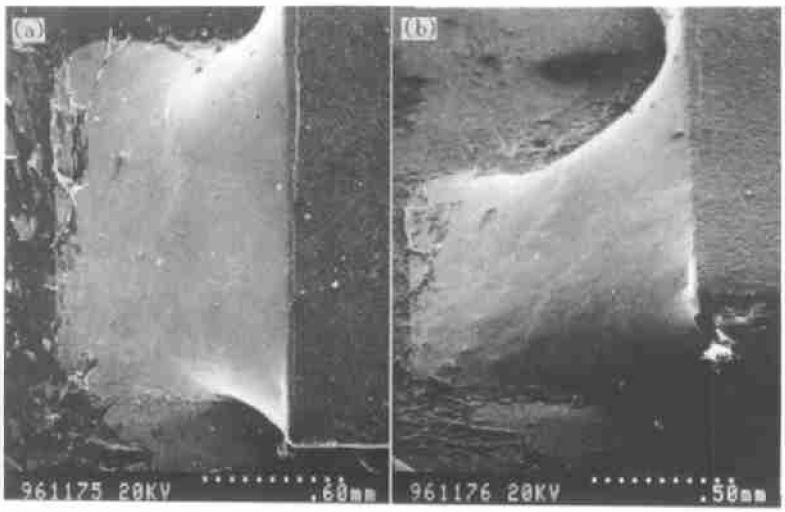

Fig.2 Micrographs of actual castellated 3-D solder joint geometry
(a)—Up view; (b)—Side view

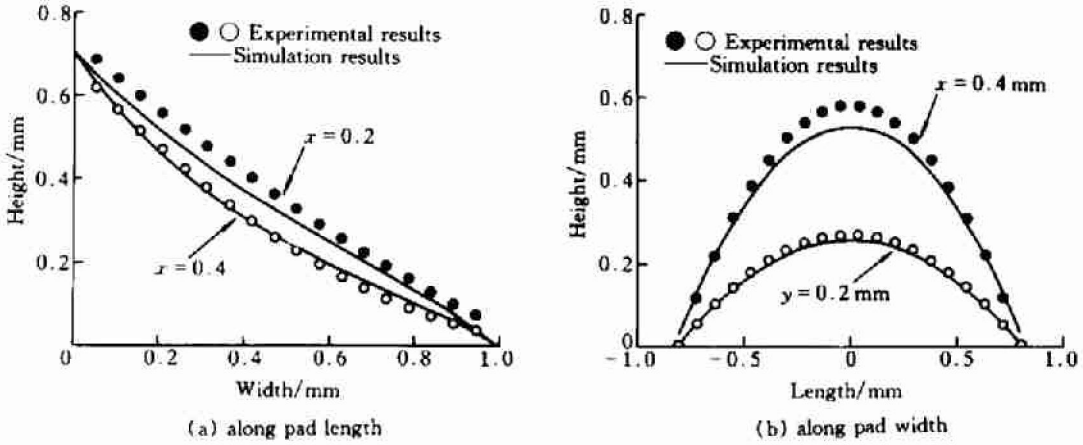

(a) along pad length (b) along pad width

Fig.3 Comparison between simulated and experimental results of 3-D solder joint geometry (solder volume = 0.4 mm^3)

in the conjunction, solder volume, surface tension and density of molten solder, and wetting angles on metallization surfaces. The properties of molten tin-based solder are taken as $\rho = 8.34$ g/cm^3 and $\gamma = 0.49$ N/m[3,12]. All calculation are on the basis of a gravitational acceleration $g = 9.81$ m/s^2. The wetting angle of molten eutectic solder on Cu surface is determined to be 15° from the experimental in this paper, which is near the value in Ref. [3]. In this paper, the solder joint geometry for two typical electronic packages, the chip component RC3216 for castellated leadless application and 100 pins thin quad flat package (TQFP) for fine pitch application, are simulated.

4.2 Simulation results

Fig.4 and Fig.5 show the simulation results

of solder joint geometry for RC3216 chip component and 100 pins TQFP, respectively. It can be seen from Fig. 4 that the castalleted solder fillet shape exhibits spatial curved surface, the solder fillets vary from concave to convex with increasing solder volume. For small solder volume, wetting and spreading of molten solder do not reach the limiting size, the contact angles are equal to wetting angles, i.e., 15°. As more solder volume is added to the joint, molten solder reaches the corresponding limiting size, resulting in big acute or even obtuse angles. It can be seen from Fig. 5 that the wetting of molten solder on the heel of gullwing type lead (outer radius of the lead) is relatively higher, or even overtops the thickness of the lead. The molten solder wets the two side walls of the lead gradually. From the above results, the established simulation method in this paper can excellently reveal the theoretical 3-D solder joint geometry in electronic package and assembly.

4.3 Comparison and discussion

Comparison between experimental results for solder joint fillet profiles and those calculated with numerical method is shown in Fig. 3. The results demonstrate that there is a good agreement. It is indicated that the numerical simulations on 3-D solder joint geometries are realistic.

Comparison of the simulation results with the present experimental results also demonstrates that the effects of heat transfer and metal reactions on solder joint geometry are not significant. From the results of Heinrich *et al*[3], the surface tension dominates gravitational force when the amount of solder is small enough. It is true in high I/O, fine pitch package and assembly application where the solder volume of each solder joint is usually only the magnitude of 10^{-2} mm^3, so the gravitational energy for solder joint geometry can be neglected. The little discrepancies between the theoretical and experimental results can be explained by Marangoni flow at high

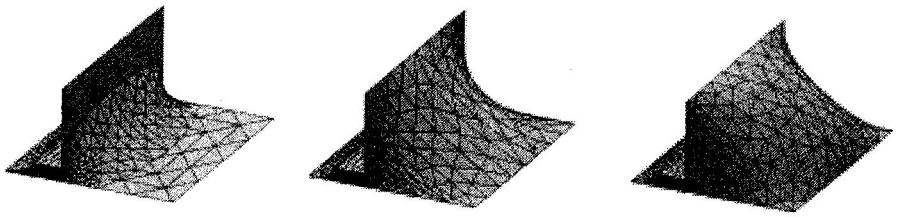

(a) $V=0.16\ mm^3$ (b) $V=0.30\ mm^3$ (c) $V=0.50\ mm^3$

Fig. 4 Simulation results of solder joint geometries for chip component

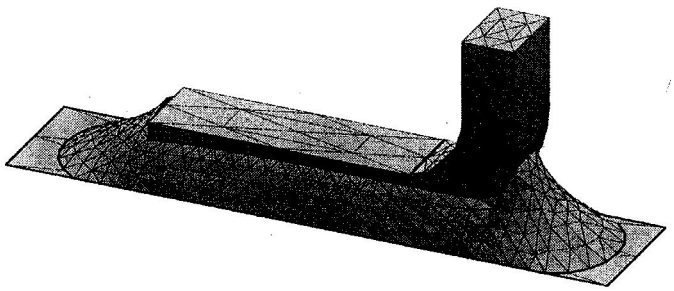

Fig. 5 Simulation result of solder joint geometry for TQFP

temperatures[14]. Oxidation and flux effects are other potential sources that should be investigated in future study.

5 APLLICATION IN SOLDER JOINT RELIABILITY

5.1 Thermal cycle test

The specimen consists of chip component and FR4 substrate where the chip component was mounted with eutectic solder at both ends. By varying the design parameters, the different solder joint geometry was obtained with reflow soldering process. In order to investigate the influences of solder joint geometry on the solder joint reliability, the specimens were tested under thermal cycle loading.

A T-2427 SX Precision Temperature Forcing system (PTFs) was applied to thermal cycling. The MIL-STD-88 method was used for thermal cycling test: temperature range -55 ℃ $\sim +125$ ℃, dwell time 15 min at both peak temperatures, ramp up/down rate 12 ℃/min and cyclic frequency 1 cycle/h. Because there is no exact standard failure criterion for solder joint under thermal cycling, the failure criterion in the present study was that the length of crack propagation penetrates 80% of the whole joint.

5.2 Results

Table 1 lists the experimental results of thermal cycling tests. In order to classify solder joint shape with different thermal cycle lives, the contact angles on substrate pad and metallization cap of chip component are used. The contact angle equals the wetting angle for more concave solder fillet shape, 15°~35° for concave, ~45° for flat, 55°~75° for convex and >75° for more convex, respectively. The distribution of thermal cycle numbers of the same solder joint geometry can follow the Weibull cumulative distribution function, that is,

$$F(c) = 1 - \exp(-c/\alpha)^{\beta} \quad (14)$$

where c is the thermal cycle number to fail, α is the scale parameter, and β is the Weibull slope, respectively. The parameters of the Weibull function were obtained with least square fitting method. Fig.6 shows the thermal cycling lives distribution of solder joints. The mean thermal cycle life (N_f^*) corresponding to each solder joint geometry can be obtained with 50% probability of failure (i.e., $F(c)=50\%$). The results show that the solder joint geometry has important influence on the solder joint reliability. The thermal cycle life for the concave solder fillet with relatively small solder volume is very low (~ 50 cycles), the thermal cycle lives for flat and convex solder fillet is increased

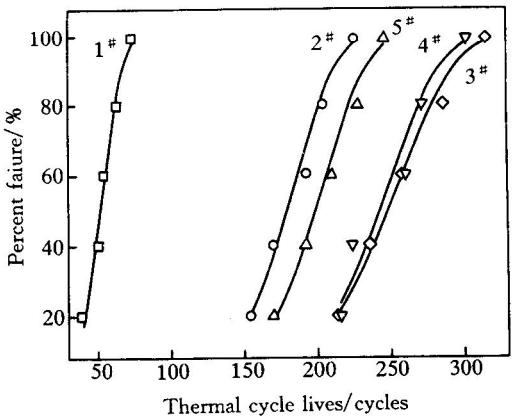

Fig.6 Weibull failure distribution of solder joints under thermal cycling

Table 1 Design parameters for solder joint geometry and thermal cycle lives

Sample series	Solder volume /mm³	Solder fillet shape	Number of thermal cycle failure, cycles					Mean life N_f^* /cycles
			1	2	3	4	5	
1#	0.2	More concave	74	56	40	52	64	53
2#	0.3	Concave	170	192	154	204	226	180
3#	0.4	Flat	236	214	258	286	316	250
4#	0.5	Convex	216	224	272	260	302	243
5#	0.7	More convex	192	170	228	210	246	200

* Other design parameters for solder joint geometry are fixed: the pad length is 0.8 mm and the stand-off height is 0.1 mm.

effectively (~240 cycles).

The analysis of solder joint reliability could be linked to the solder joint geometry. By using the finite element method, the stress/strain responses, the damage process during thermal cycling can be numerically simulated. These results are very useful for optimal design of solder joint and can give valuable information for manufacturing process. Those results will be published elsewhere.

6 CONCLUSIONS

(1) The potential energy controlling equation for SnPb solder joint geometry was established. The solder joint geometries of chip component and thin quad flat package were simulated with finite element method. The simulation results are coincident well with the experimental results, the simulations on solder joint geometry are realistic.

(2) The contact angle of molten eutectic 60Sn40Pb solder wetting on Cu metallization is dependent on the soldering process, the coefficients in Arrihenius function for contact angle were determined.

(3) The thermal cycling tests of solder joint for chip component RC3216 revealed that the solder joint geometry plays an important role in solder joint reliability, design and control of solder joint geometry is an effective method to improve the solder joint reliability.

REFERENCES

1 Charles H K and Clatterhaugh G V. ASME J Electronic Packaging, 1990, 112(6): 135~146.
2 Sherry W M. IEEE Trans CHMT, 1985, 8(4): 417~426.
3 Heinrich S M, Elkouh A F, Nigro N J *et al*. ASME J Electronic Packaging, 1990, 112(6): 210~218.
4 Gu Y G and Li D Q. J Chemical Engineering of Japan, 1997, 30(2): 302~310.
5 Deering S E and Szekely J. J Electronic Materials, 1994, 23(12): 1325~1331.
6 Renken F P and Subbarayan G. ASME J Electronic Packaging, 1998, 120 (9): 302~308.
7 Wang G Z, Cheng Z N and Wang C Q. J Modelling Simulation Material Science Engineering, 1998, 6 (4): 557~565.
8 Zhu Q N, Wang G Z and Luo L. in Proc 5th Int'l Conf on Solid-State and Integrated Circuit Technology, Beijing, 1998: 554~558.
9 Klein Wassink R J. Soldering in Electronics. 2nd edn. Electrochemical Publications Ltd, 1989.
10 Brakke K A. Surface Evolver Manual, Version 1.95d, Susquehanna University, 1994.
11 Cheng G G and Liao N B. Trans Nonferrous Met Soc China, 1998, 8(3): 510~515.
12 Hwang J H. Solder Paste in Electronic Packaging, Van Nastrand Reinhold, New York, 1989: 283~290.
13 Chen X. in: Proc Materials Development in Microelectronics Conf, Montreal, 1991: 61~67.
14 Moon K W, Bottinger W J, Williams M E *et al*. ASME J Electronic Packaging, 1996, 118 (3): 174~183.

(Edited by Peng Chaoqun)